Vacuolar H^+-ATPase d2 Subunit: Molecular Characterization, Developmental Regulation, and Localization to Specialized Proton Pumps in Kidney and Bone

Annabel N. Smith,* François Jouret,‖ Sharyn Bord,† Katherine J. Borthwick,* Rafia S. Al-Lamki,† Carsten A. Wagner,¶ Deborah C. Ireland,† Valerie Cormier-Daire,# Annalisa Frattini,** Anna Villa,** Uwe Kornak,†† Olivier Devuyst,‖ and Fiona E. Karet*§

*Departments of *Medical Genetics and †Medicine and §Division of Renal Medicine, University of Cambridge, Cambridge, United Kingdom; ‖Division of Nephrology, Université catholique de Louvain, Brussels, Belgium; ¶Institute of Physiology, University of Zurich, Zurich, Switzerland; #Department of Medical Genetics, Hôpital Necker, Paris, France; **Istituto di Tecnologie Biomediche, Milan, Italy; and ††Institute for Medical Genetics, Charité University Hospital, Berlin, Germany*

The ubiquitous multisubunit vacuolar-type proton pump (H^+- or V-ATPase) is essential for acidification of diverse intracellular compartments. It is also present in specialized forms at the plasma membrane of intercalated cells in the distal nephron, where it is required for urine acidification, and in osteoclasts, playing an important role in bone resorption by acid secretion across the ruffled border membrane. It was reported previously that, in human, several of the renal pump's constituent subunits are encoded by genes that are different from those that are ubiquitously expressed. These paralogous proteins may be important in differential functions, targeting or regulation of H^+-ATPases. They include the d subunit, where d1 is ubiquitous whereas d2 has a limited tissue expression. This article reports on an investigation of d2. It was first confirmed that in mouse, as in human, kidney and bone are two of the main sites of d2 mRNA expression. d2 mRNA and protein appear later during nephrogenesis than does the ubiquitously expressed E1 subunit. Mouse nephron-segment reverse transcription–PCR revealed detectable mRNA in all segments except thin limb of Henle's loop and distal convoluted tubule. However, with the use of a novel d2-specific antibody, high-intensity d2 staining was observed only in intercalated cells of the collecting duct in fresh-frozen human kidney, where it co-localized with the a4 subunit in the characteristic plasma membrane-enhanced pattern. In human bone, d2 co-localized with the a3 subunit in osteoclasts. This different subunit association in different tissues emphasizes the possibility of the H^+-ATPase as a future therapeutic target.

J Am Soc Nephrol 16: 1245–1256, 2005. doi: 10.1681/ASN.2004090761

The multisubunit vacuolar-type proton pump (H^+- or V-ATPase) is essential for acidification of diverse intracellular compartments in eukaryotic cells, including endosomes, lysosomes, clathrin-coated and synaptic vesicles, chromaffin granules, and the central vacuoles of plants and fungi. In addition, H^+-ATPases function to pump protons across the plasma membrane of certain cell types, one such example being the H^+-ATPases present at high density at the apical surface of α-intercalated cells in the collecting duct of the distal nephron, where vectorial proton transport is required for urinary acidification and the maintenance of acid-base homeostasis (1).

Plasma membrane H^+-ATPases also play an important role in bone resorption by osteoclasts (2). Osteoclasts form a sealed extracellular compartment (resorption lacuna) between the plasma membrane (ruffled border) and the bone surface. Large numbers of H^+-ATPases present in the ruffled border acidify this resorption lacuna, facilitating mineral solubilization and the hydrolysis of bone matrix by proteolytic enzymes such as cathepsin K (3).

The general structure of H^+-ATPases comprises two functional sectors, V_1 and V_0. The peripheral V_1 domain binds and hydrolyzes ATP, providing the energy for H^+ translocation across the integral membrane V_0 domain. The complete identity of all of the pump components has yet to be elucidated, but the structural model put forward by Nishi and Forgac (4), based mostly on studies of the bovine clathrin-coated vesicle and yeast H^+-ATPases, suggests that there are at least 13 different subunits. In this model (Figure 1), the V_1 domain (640 kD) comprises subunits A through H, in a proposed stoichiometry of $A_3B_3C_1D_1E_1F_1G_2H_1$, whereas V_0 (260 kD) contains five subunits in a possible complex of $a_1d_1c''_1(c, c')_{5-6}$, although whether the c′ subunit is present in all species is currently unclear. Another integral membrane protein, the e subunit, also referred to as M9.7 or M9.2, was recently shown to be essential for H^+-ATPase activity in yeast and is probably a functionally essential part of all eukaryotic H^+-ATPases (5).

Received September 13, 2004. Accepted February 15, 2005.

Published online ahead of print. Publication date available at www.jasn.org.

Address correspondence to: Dr. Fiona Karet, Cambridge Institute for Medical Research, Box 139 Addenbrooke's Hospital, Cambridge, CB2 2XY, UK. Phone: +44-1223-762617; Fax: +44-1223-331206; E-mail: fek1000@cam.ac.uk

Copyright © 2005 by the American Society of Nephrology

ISSN: 1046-6673/1605-1245

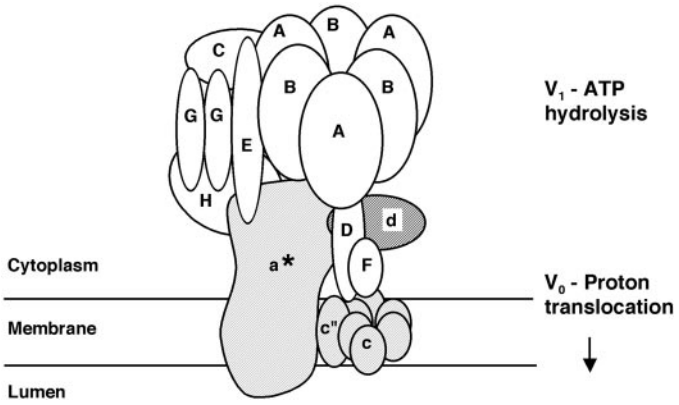

Figure 1. Schematic model of the H^+-ATPase. Adapted from reference 4. The peripheral V_1 domain subunits A through H are indicated by open symbols, and the integral membrane V_0 domain subunits a, c, and c″ are shown as gray hatched symbols, with the subject of this study, the d subunit, being indicated by darker hatching. The c′ subunit is not shown because it may not be present in all H^+-ATPases, and the e subunit was not included in this model. *The a-subunit has four different isoforms; those most relevant to this study are a3 and a4, which are present in the proton pumps found at the ruffled border of osteoclasts and the cell surface of renal intercalated cells, respectively.

The precise function(s) of many of the proton pump's subunits and the interactions between them remain undetermined. Moreover, in higher eukaryotes, several H^+-ATPase subunits have recently been shown to have multiple isoforms encoded by different genes and with differing tissue expression patterns, as summarized in Table 1. These include the B, C, E, G, a, d, and e subunits (6–12). The existence of different subunit isoforms may play an important role in the localization and activity of proton pumps in specific cell types and subcellular compartments. In support of this hypothesis, we showed previously that in human, mutations in the genes encoding B1 and a4, isoforms of the B and a-subunits that are predominantly expressed in the apical proton pumps of α-intercalated cells in the kidney, cause autosomal recessive distal renal tubular acidosis (RTA) (13,14). Similarly, autosomal recessive osteopetrosis (ARO) can be caused by mutations in a3 (15,16), a different isoform of the a-subunit that is chiefly expressed in proton pumps at the ruffled border of osteoclasts. These observations suggest that the normal functioning of some specialized types of H^+-ATPase is dependent on the presence of particular subunit isoforms, which cannot be substituted fully by a different isoform of the same subunit.

We showed previously that in human, the d2 subunit gene is expressed predominantly in kidney and osteoclasts, whereas d1 is ubiquitously expressed (10). We now report an investigation into the distribution of d2 in kidney and bone. We also analyzed the expression of the d2 subunit during mouse and human nephrogenesis and compared this with expression of the ubiquitously expressed d1 and E1 subunits, as well as with a3.

Materials and Methods

Ethical Approval

All tissues were procured with appropriate institutional ethical approval (Addenbrooke's Hospital Local Research Ethics Committee, Université catholique de Louvain Ethical Review Board).

Reverse Transcription–PCR

Total RNA was prepared from freshly harvested mouse tissues using TRIzol Reagent (Invitrogen, San Diego, CA) by standard methods. Two micrograms each of kidney, liver, testis, bone, brain, heart, skeletal muscle, lung, spleen, and thymus RNA was treated with RQ1 RNase-free DNase I (Promega, Madison, WI) and then reverse-transcribed using Super RT (HT Biotechnology Ltd, Cambridge, UK) and oligo $p(dT)_{18}$ (New England BioLabs, Beverly, MA) as primer according to the manufacturer's protocol. An aliquot of each cDNA preparation was used as template for PCR with the following primers: *Atp6v0d1*, AGCAGATGGAGGCTGTGAACATC and ACACCAAAATGGAACTGGTTCAGG; *Atp6v0d2*, CAGAGATGGAAGCTGTCAACATTG and ACACCATAATGGAATTGCCTGTTG. These primers lie in exons 3 and 8 of both *Atp6v0d1* and *Atp6v0d2*, and the expected products are 535 and 532 bp in size, respectively. For confirming successful reverse transcription, a 540-bp fragment of β-actin was amplified in parallel using the primers GTGGGCCGCCCTAGGCAC and CTCTTTGATGTCACGCACGATTTC. In each experiment, sterile water was used as template to provide a negative control. Reverse transcription reactions performed in the absence of enzyme provided a negative control sample for each tissue (data not shown). PCR fragments were resolved by electrophoresis in a 2% agarose gel.

Nephron Segment Isolation and Reverse Transcription–PCR

C57BL/6J mice (male, 25 to 30 g; Jackson Laboratory, Bar Harbor, ME) were anesthetized with ketamine and perfused through the left ventricle with PBS that contained 250 μg/ml collagenase (Sigma, St. Louis, MO). The kidneys were rapidly removed, and coronal slices 2 to 3 mm thick were cut and incubated in PBS/collagenase at 37°C for 15 min. After rinsing with ice-cold PBS, nephron segments were hand-dissected and placed in TRIzol. Total RNA was extracted and reverse-transcribed as described above. An aliquot of each cDNA preparation was amplified by PCR using the *Atp6v0d2* primers shown above. A 452-bp fragment of glyceraldehyde-3-phosphate dehydrogenase (G3PDH) was amplified in parallel using the primers ACCACAGTCCATGCCATCAC and TCCACCACCCTGTTGCTGTA. In each experiment, sterile water was used as template to provide a negative control.

Polyclonal Antisera

Two peptides, one containing 13 internal residues of human d2 (amino acids 67 to 79; VSKIDTEMRKRLC, peptide 1) and one corresponding to the C terminal 17 residues (amino acids 334 to 350; CISQRHRTKINSYIPIL, peptide 2) were synthesized, conjugated to keyhole limpet hemocyanin, and used to raise a guinea pig polyclonal antiserum, designated SK20 (Eurogentec, Seraing, Belgium).

Western Blot Analysis

Western blot analysis was carried out by standard methods, using nonfat dried milk as the blocking agent, and SK20 antiserum, either at 1:1000 dilution or 1:50, after affinity purification against peptide 2. Preimmune serum from the same animal was used as a control. Extracts of human renal cortex, rat and mouse whole kidney, and mouse brain were prepared by grinding up 0.5 to 1.0 g of snap-frozen tissue under liquid nitrogen, transferring to homogenization buffer (10 mM Tris, 150 mM NaCl, 2 mM PMSF, 1 mM EGTA, 1 mM EDTA, and 1 mM DTT,

Table 1. Mammalian H$^+$-ATPase subunits expressed at specialized sites in kidney and bone[a]

Subunit	Tissue	Species	mRNA	Protein	Evidence for Presence in Specialized H$^+$-ATPase		References
					Technique	Site	
B1	Kidney	Human	√	√	IL	IC plasma membrane (co-localizes with a4)	13,14,35
		Mouse	√	√	IL	IC plasma membrane	26,29
					Co-IP (C2, G3, a4, d2)	Kidney membranes	26
		Bovine	√	√			6
		Rat		√	IL	IC plasma membrane	6
	Inner ear	Human	√				13
		Mouse		√	IL	Endolymphatic sac/ cochlea	13
	Placenta	Human	√				35
	Male genital tract	Mouse	√	√	IL	Epididymis	29
		Rat		√	IL	Epididymis/vas deferens	36
	Eye	Rat		√	IL	Ciliary epithelium	37
		Rabbit		√	IL	Ciliary epithelium	37
C2	Kidney	Human	√				10
		Mouse (C2b)	√	√	IL	IC plasma membrane	11,26
					Co-IP (B1)	Kidney membranes	26
	Placenta	Human	√				10
	Lung	Mouse (C2a)	√	√	IL	Type II alveolar cells	11,26
G3	Kidney	Human	√				10
		Mouse	√	√	IL	IC plasma membrane	11,26
					Co-IP (B1)	Kidney membranes	26
a3[b]	Bone	Human	√	√	IL	Osteoclasts (co-localizes with d2[c])	15,24,38
		Mouse	√	√	IL	Osteoclasts	22,25,39,40
		Rabbit	√		ISH	Osteoclasts	41
a4	Kidney	Human	√	√	IL	IC plasma membrane (co-localizes with B1, d2[c])	14,21
		Mouse	√	√	IL	IC plasma membrane	7,8,21,26
					Co-IP (B1, B2)	Kidney membranes	26
	Inner ear	Human	√				42
		Mouse		√	IL	Endolymphatic sac	43
	Male genital tract	Mouse		√	IL	Epididymis/vas deferens	8,21
d2[b]	Kidney	Human	√	√	IL	IC plasma membrane (co-localizes with a4[c])	10
		Mouse	√ [c]	√	IL	IC plasma membrane	11,26,33
					Co-IP (B1)	Kidney membranes	26
	Bone	Human	√	√	IL	Osteoclasts (co-localizes with a3[c])	10
		Mouse	√ [c]				
	Lung	Human	√				10
		Mouse	√ [c]				33

[a]Co-IP, co-immunoprecipitation; IL, immunolocalization; ISH, *in situ* hybridization; IC, intercalated cells.
[b]mRNA has been observed at low levels in more widespread distribution.
[c]This study.

with one Complete Mini EDTA-free Protease Inhibitor Cocktail tablet [Roche, Lewes, UK] per 10 ml of buffer), homogenizing at 15,000 rpm with a Polytron homogenizer (Kinematica, Basel, Switzerland) for 1 min, and centrifuging at 1000 × *g* for 10 min at 4°C. For separating membrane and cytosolic fractions, supernatants were centrifuged further at 100,000 × *g* for 1 h at 4°C. Extracts of human cancellous bone were prepared by shaking fragments of bone tissue, snap-frozen in liquid nitrogen, at 2500 rpm for 2 min using a Mikro-Dismembranator S homogenizer (B. Braun Biotech, Melsungen, Germany). The crushed bone was resuspended in homogenization buffer and centrifuged as above. Protein concentrations were determined using the BioRad Protein Assay kit (Hercules, CA), and 30 or 40 μg of each was used for PAGE.

Osteoclast Culture

CD14-positive monocytes were isolated from peripheral blood of normal volunteers by magnetic bead sorting (Millenyi Biotec, Sunnyvale, CA) according to the manufacturer's protocol. For generating osteoclasts, cells were cultured in α-MEM supplemented with 10% FCS (Invitrogen), human recombinant M-CSF (25 ng/ml; R&D Systems, Abingdon, UK), and human recombinant soluble RANKL (50 ng/ml; Insight Biotechnology, Wembley, UK) on Osteologic calcium phosphate–coated slides (BD Biosciences, Oxford, UK) for 7 d at 37°C in 5% CO_2. Cells then were either prepared for immunofluorescence analysis by washing in PBS; fixing in 4% paraformaldehyde; permeabilizing using 0.1% Triton X-100; and staining for a3, d2, and vitronectin receptor (VNR) as described below or stained using Diffquik (Baxter, McGaw Park, IL) to identify osteoclasts and resorption pits. Diffquik-stained cells were visualized on a Nikon E800 microscope, and images were captured using a Basler camera.

Immunolocalization

Samples of normal human kidney were obtained from the unaffected portions of nephrectomy specimens removed for renal tumors. Samples were snap-frozen in Tissue-Tek O.C.T Compound (Sakura FineTek Europe, Zoeterwoude, The Netherlands), using isopentane cooled over liquid nitrogen. Serial 7-μm frozen cryostat-cut sections were placed on poly-L-lysine-coated (BDH) (Dagerham, UK) slides and stored at −80°C until use.

Neonatal ribs were collected post mortem from infants who were born at full term with no evidence of growth retardation or skeletal abnormalities. Ribs were immediately placed on ice and then embedded in 5% polyvinyl alcohol (Sigma) and snap-frozen in liquid nitrogen. Serial 9-μm frozen sections were cryostat-cut and picked off onto 2% 3-aminopropyltriethoxysilane–coated (Sigma) slides, air dried for 15 min, and stored at −80°C until use.

Sections were permeabilized with 100% methanol for 5 min at −20°C and washed twice with PBST (1× PBS, 0.01% Tween 20). Sections were incubated in 0.5% BSA/PBST for 15 min at room temperature, before primary antibody was applied overnight at 4°C. Primary antibodies were diluted in 0.5% BSA/PBST as follows: Guinea pig anti-human d2 (SK20) or preimmune serum 1:100; affinity-purified SK20 1:3; rabbit anti-human a3 1:1000 (gift of Jan Mattsson, AstraZeneca, Mölndal, Sweden); rabbit anti-human a4 (RA2922 [14]) 1:3000; rabbit anti-rat/mouse aquaporin-2 1:100 (Chemicon International, Temecula, CA); rabbit anti-OKP cell (opossum) megalin 1:500 (gift of Daniel Biemesderfer, Yale University); and mouse monoclonal 23C6 anti-human VNR 1:5 (gift of Mike Horton, University College London). Sections were washed three times with PBST before the following secondary antibodies (Molecular Probes, Eugene, OR) were applied at 1:250 dilution in 0.5% BSA/PBST for 1 h at room temperature: Goat anti-guinea pig Alexa 488, goat anti-rabbit Texas Red, and goat anti-mouse Alexa 568. After sections were washed three times with PBST, they were mounted with VECTASHIELD Mounting Medium with DAPI (Vector Laboratories, Burlingame, CA) and viewed using either a Zeiss Axiovert 200M fluorescence microscope and Improvision Openlab Volume Deconvolution software or a Zeiss LSM510 META confocal microscope.

Nephrogenesis Studies

Samples from human fetal kidneys, ranging from 12 to 25 wk of gestation, neonatal kidney at 4 mo, and adult kidney were obtained from the International Institute for Advancement of Medicine (Philadelphia, PA) and the Anatomic Gift Foundation (Woodbine, GA). Mouse kidney samples were obtained from CD-1 mice (Iffa Credo, Brussels, Belgium). Pregnant mice were killed by cervical dislocation. Embryos were removed and microdissected to isolate kidneys. Embryos from four different litters (average 12 embryos/litter) were collected every day from embryonic day 13.5 (E13.5) until day 5 after birth (newborn). Comparative studies were performed with four adult male kidneys.

Mouse kidney samples were homogenized in TRIzol, and total RNA was extracted and reverse-transcribed as described above. For semiquantitative reverse transcription–PCR (RT-PCR), cDNA preparations were amplified using the following primers: *Atp6v0d2*, CTTGAGTTTGAGGCCGACAG and TTGAGCTAACAACCGCAACC; *Atp6v0d1*, GCCAGCTTCCTGGACTTCAT and ACAGCCTCCATCTGCTCAAA; *Atp6v1e1*, GGCGCTCAGCGATGCAGATGT and CAAGGCGACCTTTCTCAATG; and *Atp6v0a3*, TGCTCATGGGTCTGTTCTCC and CATGGAGTGCTGGGACAGAT, which give products of 138, 143, 134, and 149 bp, respectively. A 177-bp fragment of G3PDH was amplified in parallel using primers TGCACCACCAACTGCTTAGC and GGATGCAGGGATGATGTTCT. PCR conditions were 94°C for 5 min followed by 35 (d2 subunit), 32 (d1 subunit), 33 (E1 subunit), 35 (a3 subunit), and 30 (G3PDH) cycles of 30 s at 95°C, 30 s at 61°C, and 1 min at 72°C. Negative controls included non–reverse-transcribed RNA samples and sterile water.

Real-time PCR analyses (iCycler iQ System; BioRad) were performed in duplicate using the primers shown above and iQ SYBR Green Supermix as described previously (17). PCR mixtures contained 10 nM fluorescein for initial well-to-well fluorescence normalization. PCR conditions were as follows: 94°C for 3 min followed by 40× (30 s at 95°C, 30 s at 61°C, and 1 min at 72°C). The melting temperature of each PCR product was established by recording SYBR Green fluorescence increase upon slowly renaturing DNA at the end of PCR. For each assay, standard curves were prepared by serial four-fold dilutions of mouse adult kidney cDNA. Relative mRNA expression of the d2, d1, E1, and a3 subunits was investigated in four adult male kidneys, after normalization to G3PDH: Ratio = $2^{\Delta Ct\,(G3PDH-Target\,Gene)}$. At each embryonic stage, mRNA levels of the different subunits were adjusted to the G3PDH mRNA level, and relative changes in mRNA levels during ontogeny were determined by comparison to the adult level (taken as 100%) using the following formula: Ratio = $(Efficiency_{target})^{\Delta Ct(Adult-sample)}/(Efficiency_{G3PDH})^{\Delta Ct\,(Adult-sample)}$ (18).

Kidney membrane extracts were prepared for Western blot analysis as described previously (19). Immunoblotting was carried out by standard methods, using a mouse mAb against the bovine E1 subunit (gift of Stephen Gluck, Gainesville, FL) at a 1:100 dilution and guinea pig anti-human d2 (SK20) at a 1:1000 dilution. Normalization for β-actin was obtained after stripping the blots and reprobing with a mouse monoclonal anti–β-actin antibody (Sigma). All immunoblots were performed at least in duplicate.

Screening of ARO Kindreds

With appropriate local ethical approval, genomic DNA from the affected index cases of 25 ARO kindreds and one with coexistent osteopetrosis and RTA was prepared from whole blood by standard procedures (20). All exons of the *ATP6V0D2* gene were individually amplified by PCR, using primers designed from intronic sequences flanking each exon. PCR products were sequenced using BigDye Terminator v3.1 Cycle Sequencing (Applied Biosystems, Foster City, CA).

Results

Expression Profile of the Murine d2 Subunit

We first used RT-PCR analysis to assess the gene expression profiles of the d1 and d2 subunit isoforms in a panel of 10 mouse tissues (Figure 2A). This demonstrated that the d1 isoform is ubiquitously expressed, whereas d2 is predominantly expressed in kidney, bone, and lung. The d2 isoform is also expressed at apparently lower levels in thymus, skeletal muscle, heart, and liver, although it must be noted that the assay is not quantitative. These findings are broadly in agreement with those seen previously in human, where d2 was expressed chiefly in kidney and osteoclasts (10).

Mouse Nephron Segment–Specific RT-PCR

To investigate the renal distribution of d2, we used RT-PCR to examine d2 expression in defined tubule segments prepared from mouse kidney as described previously (21). As shown in Figure 2B, d2 mRNA is present in proximal tubule, cortical collecting duct, outer medullary collecting duct, inner medullary collecting duct, and papilla. It does not seem to be expressed in the thin loop of Henle or the distal convoluted tubule.

Antibody SK20 Specifically Recognizes the d2 Subunit

We wished to confirm the localization of d2 in kidney at the protein level and also look at the distribution of this subunit in bone. We therefore raised a polyclonal antibody (SK20) in guinea pig, directed against two regions of the human d2 protein: An internal peptide of 13 residues and one corresponding to the C terminal 17 residues. We first confirmed specificity by ELISA using SK20 with and without separate affinity purification against the immunizing peptides. Immunoblotting extracts from kidney and brain showed that SK20 recognizes a protein of approximately 40 kD, corresponding to the predicted size of d2, in human kidney membrane extract but not kidney cytosol (Figure 3A). No d2 signal was seen using preimmune serum from the same animal (data not shown). Both crude and affinity-purified SK20 also cross-reacted with d2 in mouse and rat kidney membrane (Figure 3B). No band corresponding to d2 was seen in mouse brain membrane extract (data not shown). This is consistent with the RT-PCR analysis and, importantly, indicates that SK20 does not cross-react with the ubiquitously expressed d1 isoform.

Immunolocalization of d2 in Human Kidney

SK20 was used to localize d2 in unfixed frozen human kidney sections. High-intensity d2 staining was seen at the apical surface of intercalated cells in both cortical and medullary collecting ducts, with some appearing intracellularly. This appearance of d2 co-localized completely with a4 staining (Figure 4, A and B), confirming the cell type. No d2 staining was seen in cells that were positive either for the principal cell marker aquaporin-2 (Figure 4D) or for the proximal tubule marker megalin (Figure 4E). Specificity of the d2 staining was confirmed by its absence when preimmune serum from the same animal was substituted (Figure 4C).

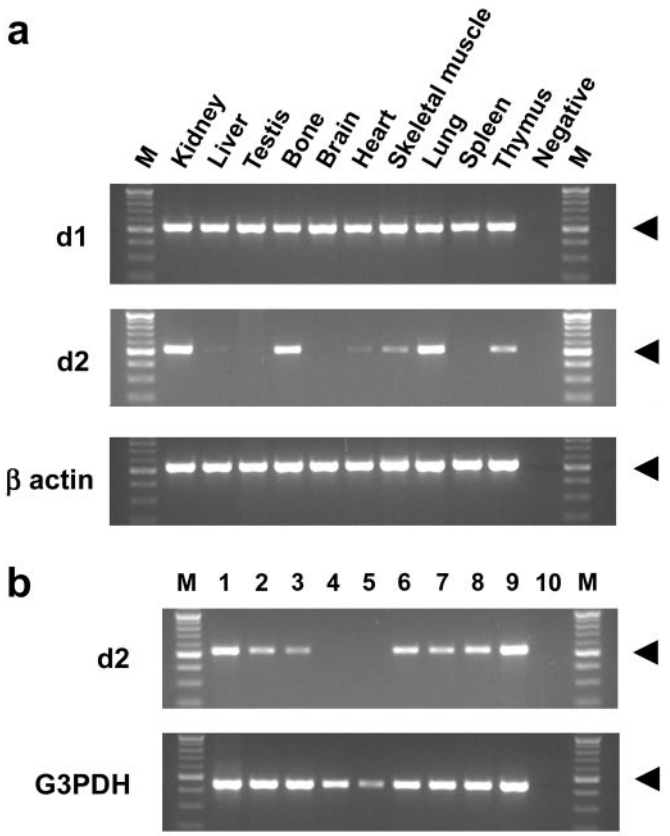

Figure 2. Reverse transcription–PCR (RT-PCR) amplification of d1 and d2 subunit mRNA from mouse tissues. (A) PCR amplification of cDNA from 10 mouse tissues was performed using gene-specific primers. *Atp6v0d1* (535-bp product) is expressed in all tissues. In contrast, *Atp6v0d2* (532 bp) is expressed chiefly in kidney, bone, and lung. β-Actin–specific primers generated a 540-bp product in all tissues, confirming successful reverse transcription. Water replaced cDNA as a negative control. Size markers (M) are in increments of 100 bp; arrowheads indicate the 500-bp band. (B) PCR amplification of *Atp6v0d2* was performed using cDNA prepared from defined segments of the mouse nephron: Total kidney (lane 1), proximal tubule S1 with glomerulus (lane 2), proximal tubule S1-S3 (lane 3), thin loop of Henle (lane 4), distal tubule (lane 5), cortical collecting duct (lane 6), outer medullary collecting duct (lane 7), inner medullary collecting duct (lane 8), papilla (lane 9), and negative control (lane 10). *Atp6v0d2* mRNA (532-bp product) is present in all of the segments studied except the thin limb of Henle's loop and distal tubule. Glyceraldehyde-3-phosphate dehydrogenase (G3PDH)-specific primers generated a 452-bp product in all tubule segments, confirming successful reverse transcription. Size markers (M) are in increments of 100 bp; arrowheads indicate the 500-bp band.

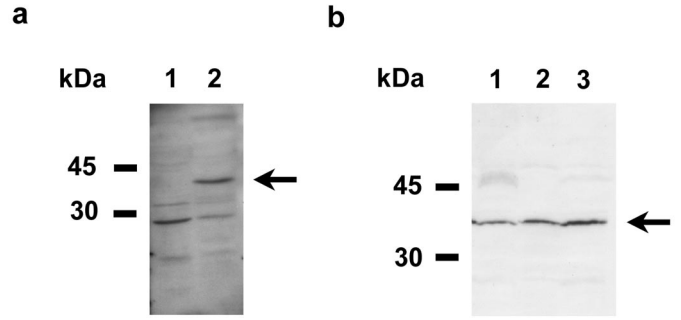

Figure 3. Western blot analysis of d2 expression in kidney extracts. (A) immunoblotting of human kidney cytosol (lane 1) and human kidney membrane (lane 2). The guinea pig polyclonal antibody SK20 recognizes a protein of approximately 40 kD (indicated by the arrow), corresponding to the predicted size of d2, in human kidney membrane extract but not in kidney cytosol. (B) Immunoblotting, using affinity-purified SK20, of human kidney membrane (lane 1), rat kidney membrane (lane 2), and mouse kidney membrane (lane 3). SK20 cross-reacts with d2 in rat and mouse kidney membrane (indicated by the arrow).

Immunolocalization of d2 in Cultured Human Osteoclasts and Human Neonatal Rib Bone

We studied d2 expression in bone both *in vitro* and *ex vivo*. Primary osteoclasts that were cultured on a synthetic resorbable substrate were used to demonstrate sites of localization of d2, the H^+-ATPase a3 subunit, and the VNR (integrin $\alpha V\beta 3$), a marker of osteoclast activity. Areas of lysis of the substrate were always associated with large multinucleated cells, indicating active resorption (Figure 5A). By confocal microscopy, these large cells were identified as osteoclasts, first by their intense staining for VNR and second by their multinuclearity seen with DAPI staining (Figure 5B). VNR was widely localized in the plasma membrane, again indicative of resorptive activity. There was less VNR staining within a basal area, within which, in these same cells, a3 and d2 co-localized, adjacent to the substrate (Figure 5C). a3 is known to be present at the ruffled border of osteoclasts and in late endosomes and lysosomes (22).

The *in vivo* localization of d2 in unfixed frozen human neonatal rib bone sections was also studied using SK20. Staining was confined to osteoclasts, as confirmed by positive staining of VNR (Figure 5D). d2 signal fully co-localized with staining for a3 in these cells (Figure 5E). No specific staining was seen when preimmune serum from the same animal was substituted (Figure 5F).

Thus, d2 is co-expressed with the a4 subunit in kidney and the a3 subunit in bone. However, Northern blot and RT-PCR (23–25) have demonstrated a3 mRNA in human and mouse kidney, and immunoprecipitation data have suggested that a3 protein is expressed in mouse kidney (26). We therefore sought to determine whether d2 is also co-expressed with the a3 subunit in human renal tissue, but on no occasion did the anti-a3 antibody show a staining pattern in human kidney sections. This does not necessarily exclude low levels of a3 protein expression in kidney but suggests that it may be present only at levels that are undetectable using this antibody. Conversely, a4 immunofluorescence was not detectable in bone sections (data not shown), confirming our previous negative RT-PCR findings from both mouse and human (8 and Smith *et al.*, unpublished data).

Comparative Quantification of d2 mRNA in Adult and Developing Mouse Kidney

We conducted real-time RT-PCR studies to establish the relative expression of d2 with respect to several other H^+-ATPase subunits (d1, E1, and a3) both during mouse nephrogenesis and in adult mouse kidney. As might be expected from its limited distribution pattern, these studies showed that in mature kidney, the d2 subunit mRNA was approximately 20-fold less prevalent than was message for the E1 subunit (Figure 6, A and B) and approximately 10-fold less abundant than d1 mRNA, both of which are ubiquitously expressed. a3 subunit mRNA was also less well expressed, by approximately the same fractions.

In the developing kidney, semiquantitative (Figure 6C) and real-time (Figure 6D) PCR analyses showed detectable d2 mRNA expression at E15.5 (approximately 10% of the adult level), with a progressive increase during late ontogeny (E17.5; approximately 45%) to reach the adult level at birth. By contrast, the ubiquitous d1 and E1 subunits were characterized by earlier (E13.5) expression, but whereas E1 levels seemed stable (approximately 50% of the adult level) throughout nephrogenesis followed by a significant increase at birth, as previously observed (17), the d1 isoform gradually decreased during late ontogeny before a neo-induction at birth. Although overall levels of a3 were low in the adult kidney (Figure 6B), its ontogeny pattern was characterized by an early and stable expression at a relatively higher level (approximately 150% of the adult level), with no significant change until after birth.

We also investigated the ontogeny pattern of d2 at the protein level. Immunoblotting (Figure 6E) confirmed the later detection of d2 expression at E15.5 compared with E1, but in contrast to the mRNA data, expression of E1 was seen to increase gradually from E16.5 until birth. However, there was only a negligible increase in d2 protein expression levels during late ontogeny, which contrasts with the semiquantitative and real-time PCR analyses. Of note, the d2 immunoreactive pattern was seen as a doublet in the fetal and newborn samples, whereas only the lower molecular weight band was present in the adult sample.

Expression of the d2 Subunit during Human Nephrogenesis

The expression of the d2 subunit of the H^+-ATPase during human nephrogenesis was also investigated using immunoblotting (Figure 6F). This subunit was detected from 12 gestational weeks and showed stable expression throughout kidney organogenesis. As in mouse, d2 was detected in fetal samples as a doublet, with increasing prominence of the larger band, which was noted to persist in infancy, whereas only a single band was observed in adult kidney, corresponding to the lower molecular weight band as in mouse. The significance of this doublet and the apparent switch in size are unclear at present.

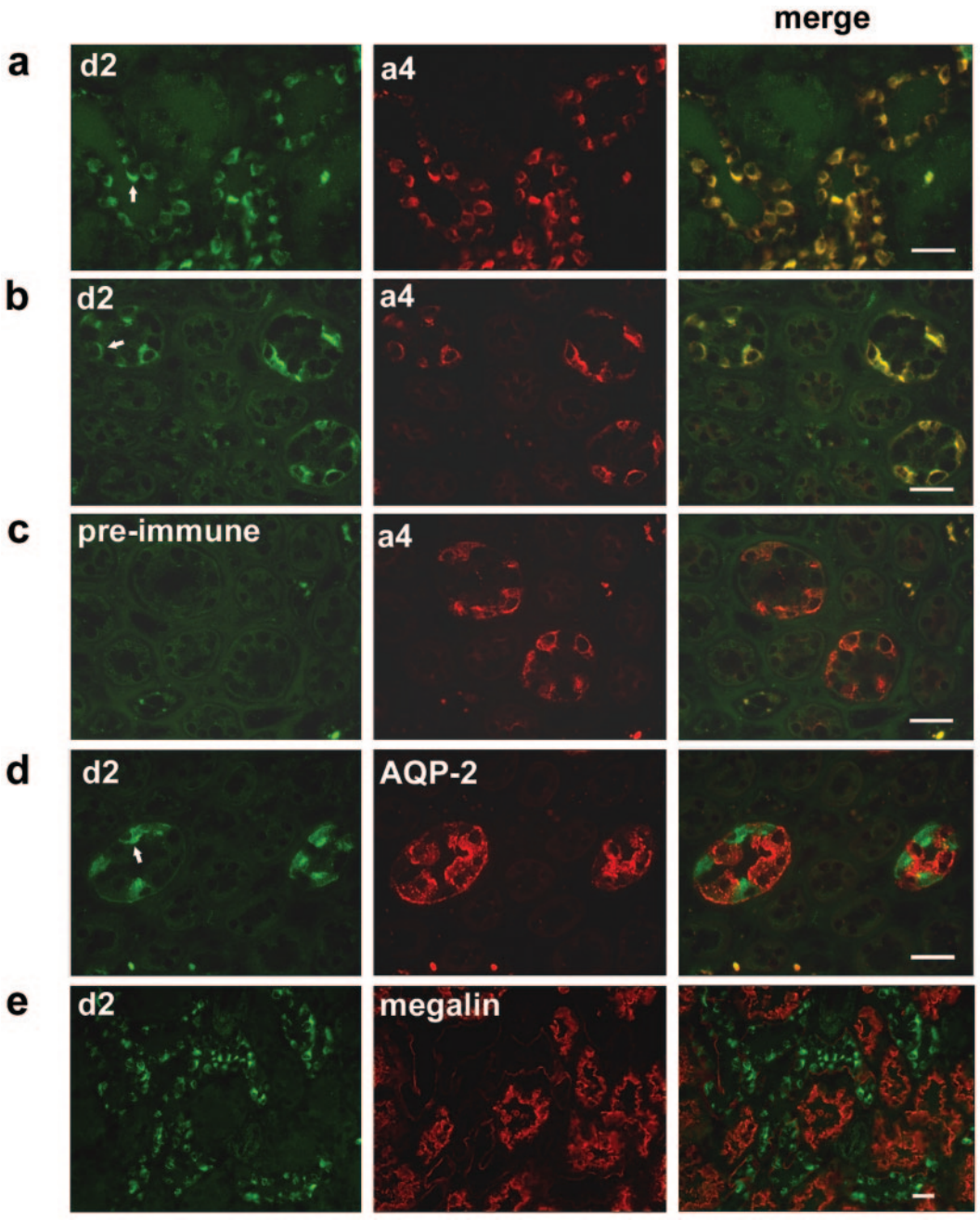

Figure 4. Immunolocalization of d2 in human kidney. SK20 was used to localize d2 in 7 μm unfixed frozen human kidney sections. Cortex (A) and medulla (B) incubated with SK20 (green) and the anti-a4 antibody RA2922 (red) reveal high-intensity d2 staining, co-localizing with a4 staining (yellow), at the apical surface of intercalated cells in the collecting duct (examples indicated by arrows). The specificity of d2 staining was confirmed by its absence when preimmune serum from the same animal was substituted (medulla; C). Confirmation of the collecting duct intercalated cell localization of d2 was provided by the absence of co-localization with either the principal cell marker aquaporin-2 (AQP-2; medulla; D) or the proximal tubule marker megalin (cortex; E). All scale bars = 25 μm.

Screening ARO Patients

Having found co-localization of d2 and a3 in osteoclasts, we proceeded to assess the candidacy of the *ATP6V0D2* gene encoding the d2 subunit as a causative gene of autosomal recessive osteopetrosis. We obtained genomic DNA from a 39-yr-old white woman who had osteopetrosis accompanied by a urine acidification defect, hypokalemia, and nephrocalcinosis and in whom normal carbonic anhydrase II levels have been found. Direct sequencing of coding exons and exon-intron boundaries of *ATP6V0D2* revealed no departures from wild-type sequence.

We also screened the gene in a cohort of 25 patients from 23 kindreds that either do not have potential disease-associated mutations in genes that are known to cause ARO, namely *TCIRG1*, *CLCN7*, and *OSTM1*, which encode the H^+-ATPase a3 subunit,

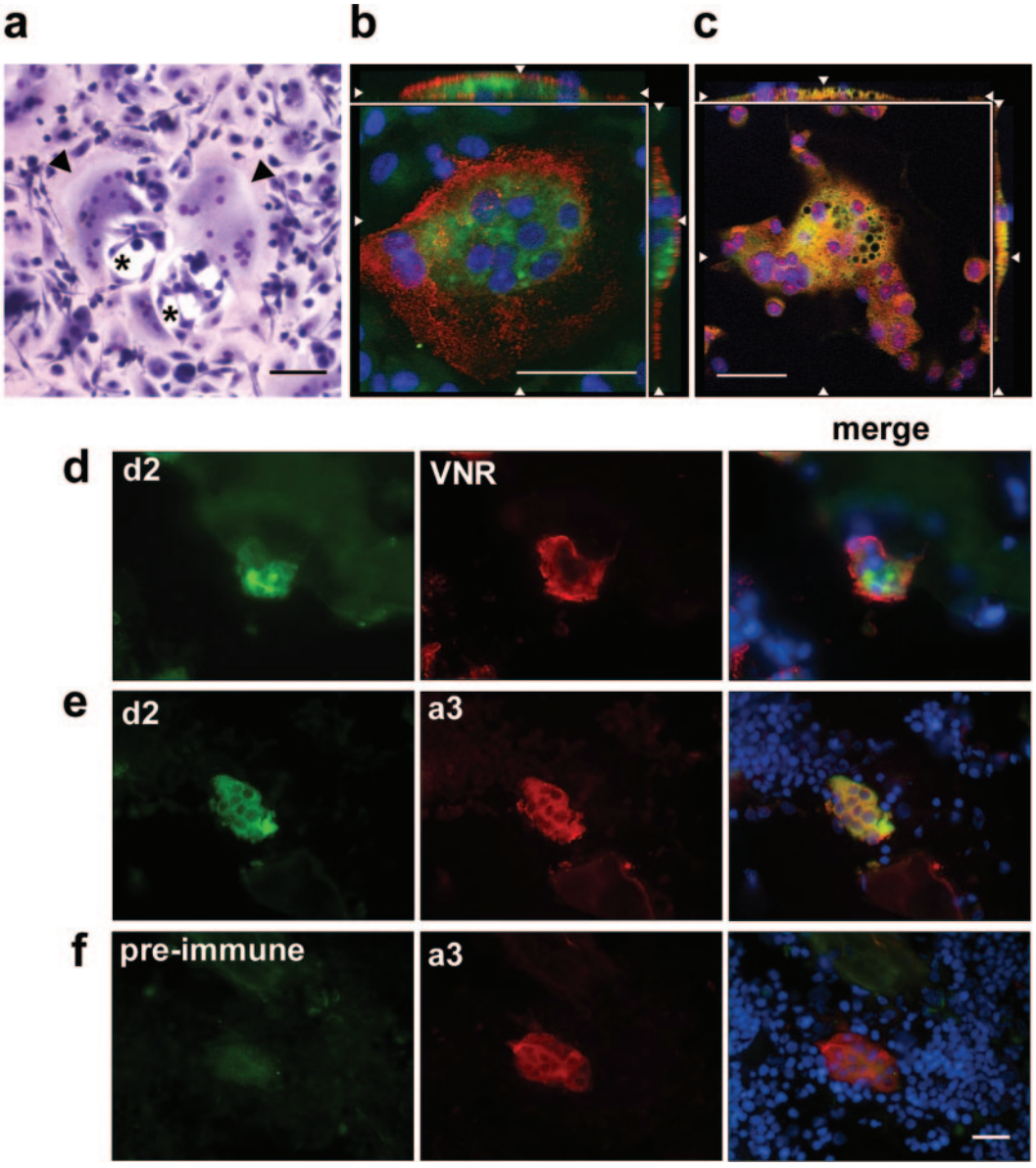

Figure 5. Immunolocalization of d2 in human cultured osteoclasts and neonatal rib bone. (A through C) Primary human osteoclasts cultured on a synthetic resorbable substrate. (A) Light microscopy reveals two large multinucleated osteoclasts (arrowheads) and associated areas of substrate lysis (*). (B and C) Merged confocal images of single osteoclasts stained for d2 (green) and one of two osteoclast markers (red): Vitronectin receptor (VNR; B) or the H^+-ATPase a3 subunit (C). Nuclei were stained using DAPI (blue). (B) VNR staining localizes to the plasma membrane, and d2 staining is seen intracellularly and in the ruffled border region, adjacent to the substrate. (C) d2 staining co-localizes with a3 (yellow). White arrowheads indicate planes of cross section. (D through F) 9-μm human frozen neonatal rib bone sections, stained for d2 and either VNR (D) or a3 (E) as above. DAPI staining demonstrates the presence of one multinucleated osteoclast per panel. As seen with cultured osteoclasts, d2 and a3 co-localize (E), with VNR staining present mainly at the cell surface (D). Specificity of d2 staining was confirmed by its absence when preimmune serum was substituted (F). All scale bars = 50 μm.

ClC-7 chloride channel, and grey-lethal protein, respectively (13 patients), or in whom only one disease-causing allele has been identified (12 patients). The affected subjects all met the clinical and biochemical criteria for the disease. RTA was absent in this group. Twenty of these patients have been previously reported (16,27,28). No potential disease-causing sequence alterations were found. This sequence analysis did identify a heterozygous single-nucleotide polymorphism (SNP), 814G→A, in exon 6 in one patient, which results in a missense alteration (G272R). As this SNP was also found heterozygously in both unaffected parents, it cannot be disease causing in isolation in the heterozygous state. We subsequently found that this SNP has recently been entered into the NCBI dbSNP database. In addition, we identified two novel intronic SNP (IVS4–12C→T and IVS5+42C→T) that were common, each being present in five patients.

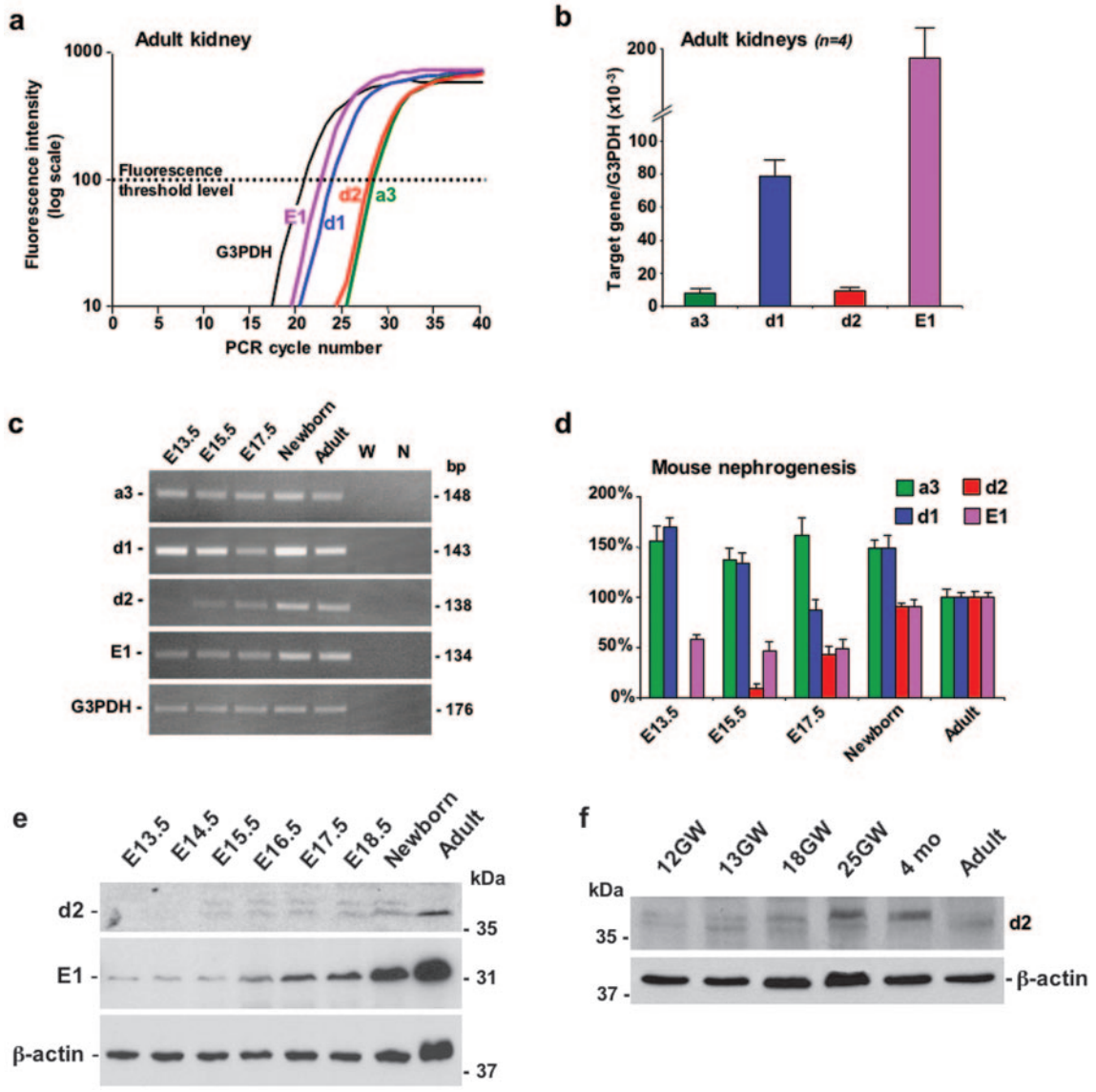

Figure 6. Comparative ontogeny of the d2, d1, E1, and a3 subunits during mouse and human nephrogenesis. (A) Representative tracings of G3PDH, a3, d1, d2, and E1 mRNA amplification by real-time RT-PCR in adult mouse kidney. (B) Comparative mRNA quantification by real-time RT-PCR of a3, d1, d2, and E1 subunits in adult mouse kidney ($n = 4$). After normalization to G3PDH, d2 and a3 were each approximately 20- and 10-fold less abundant than E1 and d1, respectively (one-way ANOVA, $P < 0.001$). (C) Representative semiquantitative PCR analysis of the expression of d2, d1, a3, E1, and G3PDH during embryogenesis (E13.5, E15.5, E17.5) and in neonatal and adult mouse kidneys. Negative controls with water (W) and non–reverse-transcribed product (N) are shown. The size of the PCR products is shown in bp. (D) Quantitative real-time RT-PCR of d2, d1, a3, and E1 mRNA expression during mouse nephrogenesis. mRNA levels were adjusted to G3PDH for each stage. The relative changes in expression during ontogeny were determined by comparison with the adult mRNA level taken as 100%. d2 mRNA is first detected at E15.5 (approximately 10% of the adult value), with a progressive increase during late ontogeny (E17.5; approximately 45%) to reach the adult expression level at birth. By contrast, ontogeny of d1 is characterized by early expression followed by a slight decrease and a neo-induction at birth, whereas E1 mRNA expression starts early during nephrogenesis and remains stable (approximately 50% of the adult value) throughout ontogeny, with a subsequent upregulation at birth. a3 shows an early (E13.5) and stable fetal expression at higher levels (approximately 150% of the adult level), without significant changes until after the neonatal period. (E) Representative immunoblots for d2, E1, and β-actin in extracts from embryonic (E13.5 to E18.5), neonatal, and adult mouse kidneys. Thirty micrograms of protein was loaded in each lane, and blots were probed with antibodies against d2, E1, and, after stripping, β-actin. The d2 subunit is detected from E15.5, with a slight increase during late ontogeny. In embryonic samples, d2 appears as a doublet, which is not found in mature kidneys. The E1 subunit is detected early during nephrogenesis and gradually increases from E16.5 until birth. (F) Representative immunoblots of d2 and β-actin in human fetal (from 12 to 25 wk gestation [GW]), 4-mo-old, and adult kidneys. The d2 subunit was detected early during human nephrogenesis at 12 wk gestation, again as a doublet. d2 expression was present throughout development, with a postnatal maturation as in the mouse.

Discussion

Our investigations of the H^+-ATPase d2 subunit confirm its limited tissue expression in mouse as well as in human. Notably, we demonstrate here that this subunit coexists with different a-subunit isoforms in the different specialized proton pumps that occur at the plasma membrane in distinct cells in kidney and in bone. This supports the idea that the existence of H^+-ATPase subunit isoforms is important for allowing the development of diverse and often specialized functions of proton pumps. Apart from G2, which is brain specific, and the a-subunit, which had already been shown to exist in a paralogous form in bone, the variance of subunit isoforms in different tissues has to date been limited to epithelia, whether in kidney, inner ear, lung, or male genital tissue. The d2 and a3 subunits are now revealed to co-localize in osteoclasts, which are of very different embryologic origin.

The polyclonal SK20 antiserum used here specifically recognizes d2 in human, mouse, and rat kidney, and it is detectable only in the membrane fraction. Our immunolocalization results in human kidney showed that d2 is present at high density at the apical pole of intercalated cells in both cortical and medullary collecting ducts, co-localizing with a4, but it is not seen in the proximal tubule. This distribution parallels previous findings for other subunits, specifically B1 in both human and rodent kidney, human a4, and the C2-b isoform in mouse (6,14,26,29). In these cases, no significant signal was observed in glomeruli or proximal and distal convoluted tubules. However, there is some discrepancy with regard to a4, where proximal staining was observed in mouse kidney (8), and it is also reported in both human and mouse renal tissue subjected to antigen retrieval techniques (21). This could be due to technical differences in fixation and retrieval and/or species-specific expression patterns. Our d2 results also show a difference between protein and nephron segment RT-PCR expression patterns, but the detection of d2 mRNA in proximal tubule by this particularly sensitive technique does not necessarily suggest the presence of d2 protein.

The murine d2 isoform can be co-immunoprecipitated from renal tissue with the B1 but not the ubiquitously expressed B2 subunit (26). Because under normal conditions it is the B1 rather than the B2 subunit that participates in the surface-destined luminal and basolateral proton pumps of α- and β-intercalated cells, respectively (6), this suggests that d2 is present only in these particular specialized proton pumps of the kidney, which in rodents also contain a4, C2-b, and G3 (7,8,26).

In contrast, further immunoprecipitation studies using mouse kidney have revealed an association between a3 and the B2 but not the B1 subunit (26). Because there is evidence to suggest that a3 mRNA is detectable in kidney in human as well as in mouse (24), we were interested to know whether a3 protein could be observed in the human kidney as well. In the event, a3 could not be seen. This suggests either a species difference or that if a3 is translated in the human kidney, it is present only at levels that are too low to permit detection.

In human bone, we observed d2 expression only in osteoclasts. These cells are more prevalent in developing bone than in adult cancellous bone, where they represent at most 1% of the cells. This explains why the signal was too weak to be visualized when SK20 was used in immunoblots of adult bone extracts (data not shown).

The presence of d2 together with a3 at the ruffled membrane and within osteoclasts may make either of these subunits attractive drug targets for the treatment of osteoporosis, but in the case of d2, this will inevitably depend on the consequences for the kidney as well. In principle, there is great potential for using H^+-ATPase inhibitors as antiresorptive therapeutics, with the caveat that compounds directed at subunits with widespread expression patterns are unlikely to be useful—such as the pharmacologically active antagonist bafilomycin used in *in vitro* studies to inhibit proton pump function. Instead, the possibility of specifically targeting the osteoclast membrane H^+-ATPase is much more attractive, as long as any therapeutic agent could be delivered efficiently to the desired site of action. Indeed, a recent publication described a compound that can discriminate between osteoclast vacuolar ATPase and lysosomal vacuolar ATPase (30).

As with the a4 subunit (17), we have found that d2 subunit expression differs temporally from the ubiquitously expressed d1 and E1 subunits during nephrogenesis in that it first appears later. This may well represent differences in the rate of maturation of different segments of the developing nephron, in that even at birth, collecting duct morphology and function are still immature. Similarly, a postnatal increase in mRNA and protein for the B1 and a4 subunits, both of which are important for collecting duct function, was reported recently (31).

We also observed a d2 doublet in fetal samples. This might be due to differential protein processing, for example by glycosylation or phosphorylation. Another possibility is that of alternative mRNA splicing, but we have observed only a single PCR product when amplifying from various cDNA.

Given the specificity of d2 expression, we regarded it as a good candidate gene for inherited osteopetrosis. We reasoned that the likeliest phenotype would include both bone thickening and a urine acidification defect, as is seen in those with *CA2* mutations (32), but also screened ARO patients who harbor one or no mutations in the known ARO genes. We have not found any disease-causing mutations in the patients who are available to us, whether with or without accompanying RTA. In view of the uncertainty about renal a3 expression in the human kidney, it is notable that no renal phenotype is reported in recessive osteopetrosis caused by *ATP6V0A3* mutations, although it is unlikely that this has been systematically sought.

The d subunit is classified as a component of the V_0 domain through protein–protein interactions rather than by integration into the membrane itself and is proposed to be present at the cytoplasmic side of the membrane. Its precise contribution to H^+-ATPase function remains unclear, although Forgac *et al.* (33) suggested that the d subunit may play a role in the coupling of ATP hydrolysis to proton transport. Recently, the crystallization of *Thermus thermophilus* subunit C, which is homologous to the eukaryotic d subunit, was reported (34). Solution of the crystal structure and its superposition onto the low-resolution electron micrograph structure of the holoenzyme, using data from cross-linking experiments, suggest that

this subunit serves as a socket to attach V_1 central stalk subunits onto the phospholipid ring of the V_0 domain, which would couple the two domains, in agreement with Forgac's model.

Acknowledgments

This work was supported by the Wellcome Trust (K.J.B., S.B., D.C.I., F.E.K., A.N.S.) and Medical Research Council (R.A.); the Swiss National Science Foundation (grant 31-68318.02 to C.A.W.); the Belgian agencies FNRS (research fellowship to F.J.) and FRSM; the Fondation Alphonse et Jean Forton and the Action de Recherches Concertées (00/05-260); and MIUR-FIRB (grant RBNE019J9W to A.V.).

Parts of this work were presented in abstract form at the American Society of Nephrology (San Diego, CA, November 14 to 17, 2003) and the UK Bone and Tooth Society (Oxford, UK, June 29 to 30, 2004).

We are grateful to Y. Cnops, H. Debaix, and Mark Bowen for excellent technical assistance. We thank Dr. S. Misler and Dr. Gul Shah (Washington University, St. Louis, MO) for provision of clinical details and for preparing DNA.

References

1. Gluck SL, Underhill DM, Iyori M, Holliday LS, Kostrominova TY, Lee BS: Physiology and biochemistry of the kidney vacuolar H^+-ATPase. *Annu Rev Physiol* 58: 427–445, 1996
2. Blair HC, Teitelbaum SL, Ghiselli R, Gluck S: Osteoclastic bone resorption by a polarized vacuolar proton pump. *Science* 245: 855–857, 1989
3. Bossard MJ, Tomaszek TA, Thompson SK, Amegadzie BY, Hanning CR, Jones C, Kurdyla JT, McNulty DE, Drake FH, Gowen M, Levy MA: Proteolytic activity of human osteoclast cathepsin K. Expression, purification, activation, and substrate identification. *J Biol Chem* 271: 12517–12524, 1996
4. Nishi T, Forgac M: The vacuolar (H+)-ATPases—Nature's most versatile proton pumps. *Nat Rev Mol Cell Biol* 3: 94–103, 2002
5. Sambade M, Kane PM: The yeast vacuolar proton-translocating ATPase contains a subunit homologous to the *Manduca sexta* and bovine e subunits that is essential for function. *J Biol Chem* 279: 17361–17365, 2004
6. Nelson RD, Guo XL, Masood K, Brown D, Kalkbrenner M, Gluck S: Selectively amplified expression of an isoform of the vacuolar H^+-ATPase 56-kilodalton subunit in renal intercalated cells. *Proc Natl Acad Sci U S A* 89: 3541–3545, 1992
7. Oka T, Murata Y, Namba M, Yoshimizu T, Toyomura T, Yamamoto A, Sun-Wada GH, Hamasaki N, Wada Y, Futai M: a4, a unique kidney-specific isoform of mouse vacuolar H^+-ATPase subunit a. *J Biol Chem* 276: 40050–40054, 2001
8. Smith AN, Finberg KE, Wagner CA, Lifton RP, Devonald MA, Su Y, Karet FE: Molecular cloning and characterization of *Atp6n1b*: A novel fourth murine vacuolar H^+-ATPase a-subunit gene. *J Biol Chem* 276: 42382–42388, 2001
9. Imai-Senga Y, Sun-Wada GH, Wada Y, Futai M: A human gene, *ATP6E1*, encoding a testis-specific isoform of H^+-ATPase subunit E. *Gene* 289: 7–12, 2002
10. Smith AN, Borthwick KJ, Karet FE: Molecular cloning and characterization of novel tissue-specific isoforms of the human vacuolar H^+-ATPase C, G and d subunits, and their evaluation in autosomal recessive distal renal tubular acidosis. *Gene* 297: 169–177, 2002
11. Sun-Wada GH, Yoshimizu T, Imai-Senga Y, Wada Y, Futai M: Diversity of mouse proton-translocating ATPase: Presence of multiple isoforms of the C, d and G subunits. *Gene* 302: 147–153, 2003
12. Ueda T, Ugawa S, Shimada S: A novel putative M9.2 isoform of V-ATPase expressed in the nervous system. *Neuroreport* 14: 25–30, 2003
13. Karet FE, Finberg KE, Nelson RD, Nayir A, Mocan H, Sanjad SA, Rodriguez-Soriano J, Santos F, Cremers CW, Di Pietro A, Hoffbrand BI, Winiarski J, Bakkaloglu A, Ozen S, Dusunsel R, Goodyer P, Hulton SA, Wu DK, Skvorak AB, Morton CC, Cunningham MJ, Jha V, Lifton RP: Mutations in the gene encoding B1 subunit of H^+-ATPase cause renal tubular acidosis with sensorineural deafness. *Nat Genet* 21: 84–90, 1999
14. Smith AN, Skaug J, Choate KA, Nayir A, Bakkaloglu A, Ozen S, Hulton SA, Sanjad SA, Al-Sabban EA, Lifton RP, Scherer SW, Karet FE: Mutations in *ATP6N1B*, encoding a new kidney vacuolar proton pump 116-kD subunit, cause recessive distal renal tubular acidosis with preserved hearing. *Nat Genet* 26: 71–75, 2000
15. Frattini A, Orchard PJ, Sobacchi C, Giliani S, Abinun M, Mattsson JP, Keeling DJ, Andersson AK, Wallbrandt P, Zecca L, Notarangelo LD, Vezzoni P, Villa A: Defects in TCIRG1 subunit of the vacuolar proton pump are responsible for a subset of human autosomal recessive osteopetrosis. *Nat Genet* 25: 343–346, 2000
16. Kornak U, Schulz A, Friedrich W, Uhlhaas S, Kremens B, Voit T, Hasan C, Bode U, Jentsch TJ, Kubisch C: Mutations in the a3 subunit of the vacuolar H^+-ATPase cause infantile malignant osteopetrosis. *Hum Mol Genet* 9: 2059–2063, 2000
17. Jouret F, Igarashi T, Gofflot F, Wilson PD, Karet FE, Thakker RV, Devuyst O: Comparative ontogeny, processing, and segmental distribution of the renal chloride channel, ClC-5. *Kidney Int* 65: 198–208, 2004
18. Pfaffl MW: A new mathematical model for relative quantification in real-time RT-PCR. *Nucleic Acids Res* 29: e45, 2001
19. Devuyst O, Christie PT, Courtoy PJ, Beauwens R, Thakker RV: Intra-renal and subcellular distribution of the human chloride channel, CLC-5, reveals a pathophysiological basis for Dent's disease. *Hum Mol Genet* 8: 247–257, 1999
20. Bell GI, Karam JH, Rutter WJ: Polymorphic DNA region adjacent to the 5′ end of the human insulin gene. *Proc Natl Acad Sci U S A* 78: 5759–5763, 1981
21. Stehberger PA, Schulz N, Finberg KE, Karet FE, Giebisch G, Lifton RP, Geibel JP, Wagner CA: Localization and regulation of the ATP6V0A4 (a4) vacuolar H^+-ATPase subunit defective in an inherited form of distal renal tubular acidosis. *J Am Soc Nephrol* 14: 3027–3038, 2003
22. Toyomura T, Murata Y, Yamamoto A, Oka T, Sun-Wada GH, Wada Y, Futai M: From lysosomes to the plasma membrane: Localization of vacuolar-type H^+-ATPase with the a3 isoform during osteoclast differentiation. *J Biol Chem* 278: 22023–22030, 2003
23. Nishi T, Forgac M: Molecular cloning and expression of three isoforms of the 100-kDa a subunit of the mouse vacuolar proton-translocating ATPase. *J Biol Chem* 275: 6824–6830, 2000
24. Scott BB, Chapman CG: The putative 116 kDa osteoclast

specific vacuolar proton pump subunit has ubiquitous tissue distribution. *Eur J Pharmacol* 346: R3–R4, 1998
25. Toyomura T, Oka T, Yamaguchi C, Wada Y, Futai M: Three subunit a isoforms of mouse vacuolar H^+-ATPase. Preferential expression of the a3 isoform during osteoclast differentiation. *J Biol Chem* 275: 8760–8765, 2000
26. Sun-Wada GH, Murata Y, Namba M, Yamamoto A, Wada Y, Futai M: Mouse proton pump ATPase C subunit isoforms (C2-a and C2-b) specifically expressed in kidney and lung. *J Biol Chem* 278: 44843–44851, 2003
27. Frattini A, Pangrazio A, Susani L, Sobacchi C, Mirolo M, Abinun M, Andolina M, Flanagan A, Horwitz EM, Mihci E, Notarangelo LD, Ramenghi U, Teti A, Van Hove J, Vujic D, Young T, Albertini A, Orchard PJ, Vezzoni P, Villa A: Chloride channel ClCN7 mutations are responsible for severe recessive, dominant, and intermediate osteopetrosis. *J Bone Miner Res* 18: 1740–1747, 2003
28. Ramirez A, Faupel J, Goebel I, Stiller A, Beyer S, Stockle C, Hasan C, Bode U, Kornak U, Kubisch C: Identification of a novel mutation in the coding region of the grey-lethal gene *OSTM1* in human malignant infantile osteopetrosis. *Hum Mutat* 23: 471–476, 2004
29. Finberg KE, Wagner CA, Stehberger PA, Geibel JP, Lifton RP: Molecular cloning and characterization of Atp6v1b1, the murine vacuolar H^+-ATPase B1-subunit. *Gene* 318: 25–34, 2003
30. Niikura K, Takano M, Sawada M: A novel inhibitor of vacuolar ATPase, FR167356, which can discriminate between osteoclast vacuolar ATPase and lysosomal vacuolar ATPase. *Br J Pharmacol* 142: 558–566, 2004
31. Bonnici B, Wagner CA: Postnatal expression of transport proteins involved in acid-base transport in mouse kidney. *Pflugers Arch* 448: 16–28, 2004
32. Sly WS, Hewett-Emmett D, Whyte MP, Yu YS, Tashian RE: Carbonic anhydrase II deficiency identified as the primary defect in the autosomal recessive syndrome of osteopetrosis with renal tubular acidosis and cerebral calcification. *Proc Natl Acad Sci U S A* 80: 2752–2756, 1983
33. Nishi T, Kawasaki-Nishi S, Forgac M: Expression and function of the mouse V-ATPase d subunit isoforms. *J Biol Chem* 278: 46396–46402, 2003
34. Iwata M, Imamura H, Stambouli E, Ikeda C, Tamakoshi M, Nagata K, Makyio H, Hankamer B, Barber J, Yoshida M, Yokoyama K, Iwata S: Crystal structure of a central stalk subunit C and reversible association/dissociation of vacuole-type ATPase. *Proc Natl Acad Sci U S A* 101: 59–64, 2004
35. van Hille B, Richener H, Schmid P, Puettner I, Green JR, Bilbe G: Heterogeneity of vacuolar H^+-ATPase: Differential expression of two human subunit B isoforms. *Biochem J* 303: 191–198, 1994
36. Breton S, Tyszkowski R, Sabolic I, Brown D: Postnatal development of H^+ ATPase (proton-pump)-rich cells in rat epididymis. *Histochem Cell Biol* 111: 97–105, 1999
37. Wax MB, Saito I, Tenkova T, Krupin T, Becker B, Nelson N, Brown D, Gluck SL: Vacuolar H^+-ATPase in ocular ciliary epithelium. *Proc Natl Acad Sci U S A* 94: 6752–6757, 1997
38. Li YP, Chen W, Stashenko P: Molecular cloning and characterization of a putative novel human osteoclast-specific 116-kDa vacuolar proton pump subunit. *Biochem Biophys Res Commun* 218: 813–821, 1996
39. Li YP, Chen W, Liang Y, Li E, Stashenko P: *Atp6i*-deficient mice exhibit severe osteopetrosis due to loss of osteoclast-mediated extracellular acidification. *Nat Genet* 23: 447–451, 1999
40. Deng W, Stashenko P, Chen W, Liang Y, Shimizu K, Li YP: Characterization of mouse *Atp6i* gene, the gene promoter, and the gene expression. *J Bone Miner Res* 16: 1136–1146, 2001
41. Manolson MF, Yu H, Chen W, Yao Y, Li K, Lees RL, Heersche JN: The a3 isoform of the 100-kDa V-ATPase subunit is highly but differentially expressed in large ($\geq$10 nuclei) and small ($\leq$5 nuclei) osteoclasts. *J Biol Chem* 278: 49271–49278, 2003
42. Stover EH, Borthwick KJ, Bavalia C, Eady N, Fritz DM, Rungroj N, Giersch AB, Morton CC, Axon PR, Akil I, Al-Sabban EA, Baguley DM, Bianca S, Bakkaloglu A, Bircan Z, Chauveau D, Clermont MJ, Guala A, Hulton SA, Kroes H, Li Volti G, Mir S, Mocan H, Nayir A, Ozen S, Rodriguez Soriano J, Sanjad SA, Tasic V, Taylor CM, Topaloglu R, Smith AN, Karet FE: Novel *ATP6V1B1* and *ATP6V0A4* mutations in autosomal recessive distal renal tubular acidosis with new evidence for hearing loss. *J Med Genet* 39: 796–803, 2002
43. Dou H, Xu J, Wang Z, Smith AN, Soleimani M, Karet FE, Greinwald JH Jr, Choo D: Co-expression of pendrin, vacuolar H^+-ATPase a4-subunit and carbonic anhydrase II in epithelial cells of the murine endolymphatic sac. *J Histochem Cytochem* 52: 1377–1384, 2004